Proposal of selective inhibitor for bacterial zinc metalloprotease: Molecular mechanics and *ab initio* molecular orbital calculations

Kyohei Imai[a], Ryosuke Saito[a], Takuya Ezawa[a], Satoshi Sugiyama[a], Ingebrigt Sylte[b] and Noriyuki Kurita[a,*]

[a] *Department of Computer Science and Engineering, Toyohashi University of Technology, Toyohashi, 441-8580, Japan*

[b] *Department of Medical Biology, Faculty of Health Sciences, UiT The Arctic University of Norway, NO-9037 Tromsø, Norway*

*** Corresponding author:**
Noriyuki Kurita, Associate Professor, Ph. D.
Toyohashi University of Technology
Department of Computer Science and Engineering
Tempaku-cho, Toyohashi, 441-8580, Japan
Tel. & Fax: 81-532-44-6875
E-mail: kurita@cs.tut.ac.jp

Abstract

The zinc metalloprotease pseudolysin (PLN) secreted from *Pseudomonas aeruginosa* degrades extracellular proteins to produce bacterial nutrition, and various types of PLN inhibitors have been developed to suppress the bacterial growth. However, as the structure of the ligand-binding pocket of PLN has large similarities to those of human matrix metalloproteinases (MMPs) and other human zinc metalloprotease, there is a risk that PLN inhibitors also inhibit human zinc proteases. In this study, we propose a novel agent that may bind stronger to PLN than to MMPs. The compound is proposed based on the specific molecular interactions between existing agents and PLN/MMP metalloproteases evaluated by the present molecular simulations. First, we confirmed that the binding energies of PLN agents evaluated using the *ab initio* fragment molecular orbital method were comparable to the IC_{50} values obtained through previous experiments. In addition, the specific molecular interactions between these agents and MMP-9 were investigated to elucidate the fact that some of the agents bind weaker to MMP than PLN. Based on the results, we proposed a novel agent and investigated its binding properties with PLN and MMP. The results may provide useful information for the development of potent inhibitors for PLN with few potential side effects in human bodies.

Keywords

Metalloprotease; Bacterial virulence; Molecular simulation; Fragment molecular orbital; Protein–ligand interactions; Drug design; Antimicrobial resistance; Selective inhibitor

1. Introduction

Bacteria are pivotal in the pathogenesis of various infectious diseases, and antimicrobial agents that inhibit the growth of bacteria have been widely used in the treatment for infectious diseases. However, prolonged use of the same agent at high concentrations increases the risk of the emergence of novel bacteria with antimicrobial resistance (AMR) against the agent. In fact, according to a 2019 report [1] from the Centers for Disease Control and Prevention in United States, more than 2.8 million antibiotic-resistant infections occur in United States each year, and more than 35,000 people die as a result. In the countries of the European Union and its economic area, the burden of deaths caused by antibiotic-resistant bacteria was estimated to be over 33,000 in 2015 [2]. It was estimated that the burden of deaths from AMR could increase to 10 million lives lost each year by 2050 unless action is taken. The number of deaths will become larger than those caused by cancer [3]. Along with human costs, AMR also has a large economical burden, which will continue to grow if resistance is not tackled [2, 3]

In bacterial pathogens, the outer membrane and active efflux pumps are the main components for reducing the susceptibility of these organisms to a number of antibiotics [4]. Accordingly, the inhibition of these components offers potential for the rejuvenation of a broad range of antibacterial agents. However, if a novel agent attacks bacteria directly to reduce its activity, there is a risk for producing mutant-type of bacteria with AMR against the novel agent. Thus, it is necessary to develop novel agents that do not attack the bacteria directly in order to reduce the risk of producing antimicrobial-resistant bacteria.

The genus *Pseudomonas* consists of more than 120 species that are ubiquitous in moist environments, such as water and soil ecosystems, and are pathogenic to plants, animals, and humans [5]. Within the *Pseudomonas* species, *P. aeruginosa* is most frequently associated with causing human infection, although it is rarely associated with causing chronic infections in previously healthy patients. However, due to the frequent use of antimicrobial agents, multidrug-resistant *P. aeruginosa* (MDRPA) was created and spread widely throughout the world. As a consequence, in 2017, the World Health Organization delivered a strong warning that *P. aeruginosa* is included in the list of the priority 1 (critical) bacteria, for which new antibiotics are urgently needed [6]. Particularly, the list highlighted the threat of MDRPA. Therefore, various therapeutic challenges associated with MDRPA were undertaken.

Pseudomonas aeruginosa secretes the virulence factor pseudolysin (PLN), which is a proteolytic enzyme of the M4 family of metalloproteases [7]. Since PLN degrades extracellular proteins and peptides that *P. aeruginosa* uses for nutrition prior to sporulation, the growth of *P. aeruginosa* may be effectively suppressed by the binding of inhibitors to the PLN active site. Novel inhibitors against PLN have therefore been developed as putative novel

antimicrobial agents [8–11]. As these agents do not attack the bacteria directly, there is a reduced risk for producing drug-resistant bacteria.

As shown in Figure S1 of the Supplementary Information (SI), PLN contains a Zn and a Ca ion [12]. The Ca ion contributes to stabilizing the PLN structure, while the Zn ion is necessary for catalytic activity and is located close to the cleavage site. The specificity of a protease is mainly determined by the topology of the active site, which contains specific binding pockets for the substrate. Binding pockets that interact with an amino acid's N-terminal for the cleavage site in the substrate are called non-prime sites (S), while the pockets binding an amino acid's C-terminal for the cleave site are called prime sites (S′). The topology of the active site is not only important for the specificity and binding of substrates, but small molecule inhibitors also interact with the Zn ion and surrounding non-prime and prime sites. In PLN, the S1' pocket includes Leu132 and Val137, and preferentially recognizes aromatic and hydrophobic amino acids, while the S2' pocket includes Asn112, Phe129, Ile186, Leu197 to recognize hydrophobic amino acids. In contrast, the S1 pocket composed of Tyr114, Trp115, and Tyr155 recognizes hydrophilic amino acids. Among these pockets, the S1' pocket was revealed to be more important for specific binding with the PLN inhibitors [13], and Arg198 located between the S1' and S2' pockets can perturb the entrance into the S1' pocket.

Matrix metalloproteinases (MMPs) comprise a family of zinc-dependent endopeptidases consisting of more than 21 human MMPs and numerous homologues from other species [14]. MMPs are synthesized as inactive zymogens and are activated by proteinase cleavage. In human bodies, MMPs play important roles in degrading extracellular matrix (ECM) proteins to produce nutrition for living cells [15]. MMPs contain Zn and Ca ions, and the Zn ion exists at the active site for degrading ECM [16]. Since the structures of the active sites of PLN and MMPs are quite similar to each other, there is a chance that an antimicrobial agent would inhibit the activities of both proteinases. As a consequence, side effects could be caused in the cellular functions of the recipient of the agent. To avoid such a tragic situation, it is necessary to develop agents that selectively inhibit PLN activity.

MMPs can promote cancer progression by increasing cancer cell growth, migration, invasion, metastasis, and angiogenesis. The expression of MMPs is often associated with poor survival. Some MMPs (e.g., MMP-7) are expressed by cancer cells, while other MMPs (e.g., MMP-2 and MMP-9) are synthesized by tumor stromal cells, including fibroblasts, myofibroblasts, inflammatory cells, and endothelial cells [17, 18]. MMP-9 was revealed to be active even at pH= 5.5 in osteoclastic cells [15]. Therefore, we employed MMP-9 (Figure S1b) as one of the target proteins in the present molecular simulations.

In a recent study [19], a novel agent (Compound 13) was developed as a potent selective inhibitor for PLN. As shown in Figure 1a, Compound 13 has a succinimide group

and binds selectively to PLN, while it does not bind strongly to MMPs such as MMP-1, MMP-2, MMP-3, MMP-7, MMP-8, and MMP-14. However, the inhibition effect of Compound 13 on MMP-9 was not elucidated. As the structures of the ligand-binding pocket of the MMP family are similar to one another, it is likely that Compound 13 cannot bind strongly to MMP-9. Therefore, Compound 13 is expected to be a potent PLN inhibitor with few risks of side effects in human bodies.

Additionally, novel Compounds 15, 50, and 51 (Figures 1b, 1c, and 1d) were synthesized on the basis of Compound 13, and their inhibitory affinities (IC_{50} values) for PLN were investigated [19]. Although their chemical structures were similar to that of Compound 13, their IC_{50} values were significantly different, as listed in Table S1 of SI. The reason for this significant difference in the IC_{50} values has not been elucidated yet.

In the present study, we first investigated the specific interactions between these compounds and PLN to elucidate the reason for the remarkable difference in the IC_{50} values of these compounds. Since PLN includes a Zn ion in its ligand-binding pocket, and the Zn ion significantly contributes to the binding between PLN and the compounds, we carefully considered the protonation states of the residues existing around the Zn ion using molecular simulations based on molecular mechanics (MM) and fragment molecular orbital (FMO) methods. Subsequently, to confirm the selective binding of Compound 13 to PLN, rather than the MMP family, we investigated the interactions between the compounds and MMP-9 in the same manner. Based on the results evaluated for PLN and MMP-9, we finally proposed a novel compound with a higher selective binding affinity to PLN, and its binding properties with regard to PLN/MMP-9 were investigated to confirm the selectivity. The present results may provide helpful information for the development of novel inhibitors that target PLN and not MMP families.

2. Details of *ab initio* molecular simulations

2.1 Constructions and optimizations of PLN/MMP-9 + compound complexes

As initial 3D structures of PLN and MMP-9, we employed the X-ray crystal structures registered in the protein data bank (PDB); their PDB IDs are 6FZX [20] and 4H3X [21], respectively. Since these structures have no information on the positions of hydrogen atoms, it is necessary to add hydrogen atoms at the appropriate positions of the protein, in order to conduct realistic molecular simulations. In fact, if hydrogen atoms are not added to the appropriate positions of the target protein, the simulated results cannot explain the results obtained by experiments, as indicated in our previous molecular simulations for the vitamin D receptor protein [22]. In addition, PLN and MMP-9 contain a Zn ion at the active site of the proteins, with histidine (His) and glutamine-acid (Glu) residues coordinated with the Zn ion.

Therefore, it is likely that the protonation states of Zn coordinating His and Glu residues have a significant effect on the specific interactions between PLN/MMP-9 and their ligands. Thus, we carefully considered their protonation states in the complexes of PLN/MMP-9 and their ligands in our present molecular simulations.

In previous molecular simulations [23−25] of the metalloprotease thermolysin (TLN), whose structure is very similar to the PLN structure, the catalytic Glu residue existing near the Zn ion was assigned to have a non-protonated Glu^- state, considering the structure around the catalytic Zn ion and the Glu residue. In addition, our previous molecular simulations [26] elucidated that Glu141 of PLN frequently occupies the Glu^- state rather than the protonated Glh-1 and Glh-2 states, whose chemical structures are shown in Figure S2 of SI. Therefore, we employed the Glu^- state for Glu141 in PLN. We assigned the same Glu^- state to Glu227 of MMP-9, which correspond to Glu141 in PLN.

The protonation states of His residues were determined based on the pKa values predicted by the PROPKA 3.1 program [27, 28]. His residues with a pKa value greater than six, and were located on the surface of the protein were assigned the Hip^+ protonation, whereas His residues with a lower pKa value located inside the protein were assigned the Hid or Hie protonation states. Figure S3 (see SI) shows the chemical structures of His residues with these protonation states. Since His residues located inside a protein can be in either the Hid or Hie state, depending on the structure of the surrounding residues, we assigned protonation states, considering the steric hindrance to the surrounding residues of PLN and MMP-9. In particular, the protonation states of His residues existing near the Zn ion were carefully determined, since their protonation states significantly affect the specific interactions between PLN/MMP-9 and their ligands.

The structures of the compounds shown in Figure 1 were optimized in vacuum by the B3LYP/6-31G(d,p) method of the *ab initio* molecular orbital calculation program Gaussian16 (G16) [29]. The charge distributions of the optimized structures were evaluated by restrained electrostatic potential (RESP) analysis [30] using the HF/6-31G(d) method of G16. Based on these charge distributions, atomic charge parameters of the force fields employed in the MM optimizations were constructed for each of the compounds. Notably, these RESP charges of the compounds are essential for accurately describing the electrostatic interactions between the compounds and the residues of PLN/MMP-9 protein in the docking as well as the MM simulations.

To produce candidate structures for the complexes between PLN/MMP-9 and the compound, we conducted molecular docking studies using AutoDock4.2.6 [31]. In the docking simulations, the size of the grid box for the docking positions was set as 1.5 times as the size of the compound, and the center of the grid box was set to the center of the ligand in the PDB

structure (PDB ID: 6FZX [20] and 4H3X [21]). The structure of the protein was fixed, while all rotatable bonds of the compound were freely rotating. The number of created candidate poses was 256, and the threshold of the root mean square distance for clustering these poses was set as 2 Å. From the various clusters generated by AutoDock, we selected clusters with the largest number of poses. The representative structures of these clusters were used in the subsequent MM and FMO calculations because there is a higher probability that the compound would possess one of the conformations contained in the cluster with a larger number of poses. It was noted that the RESP charge was assigned to each atom of the compound, while a +2 charge was assigned to Zn and Ca ions in the protein.

The representative structures of the clusters obtained from the docking simulations were fully optimized in water using the classical MM and molecular dynamic simulation program AMBER18 [32]. To properly consider the solvation effect on the complex, we added water molecules with a layer of 8 Å around the complex. The FF14SB force field [33], TIP3P model [34], and general AMBER force field [35] were assigned to the proteins, water molecules, and compounds, respectively. The criterion for the convergence of structure optimization was set as 0.0001 kcal/mol/Å.

2.2 *Ab initio* FMO calculations for the PLN/MMP-9 + compound complexes

To elucidate the specific interactions and binding affinities between PLN/MMP-9 and the compounds, we investigated the electronic properties of the complexes using the *ab initio* FMO method [36]. This method has been applied to many biomolecules to obtain accurate results comparable with experimental results. Since water molecules can contribute to the specific interactions between PLN/MMP-9 and the compounds, the water molecules existing within 8 Å of the compound were explicitly considered. The number of water molecules considered in the FMO calculations was unified for all clusters of a complex to determine the most stable cluster from the comparison of the total energies evaluated by the FMO method. Additionally, to predict the binding affinity between the compound and PLN/MMP-9, we evaluated the total inter-fragment interaction energies (IFIEs) [37] between the compound and all residues of PLN/MMP-9 using the *ab initio* FMO method [36].

In the present study, the effect of entropy on the binding affinity was not considered because a vibrational analysis for the solvated protein–compound complex is not practical when using the *ab initio* FMO method. Furthermore, the entropic effect is unlikely to be markedly different for each of the compounds, as they have quite similar chemical structures (as shown in Figure 1) and bind at the same positions of PLN or MMP-9. Thus, we investigated the total IFIEs between the compound and all residues of PLN/MMP-9 using *ab initio* FMO calculations and estimated the trends of the binding affinities under the assumption that the

entropic effects were the same for each of the compounds. In our previous study [38], the binding properties between the androgen receptor (AR) protein and its ligands were investigated using the same FMO calculations. The evaluated total IFIEs between the AR residues and the ligands were confirmed to correlate well with the binding affinities of these ligands obtained through experiments. The correlation coefficient (R^2) was 0.94 for all the nine different ligands, confirming that our evaluated total IFIEs can explain the trend of the observed binding affinities between AR and these ligands. Therefore, the present FMO calculations are expected to obtain accurate binding properties between the PLN/MMP-9 residues and the compounds.

In FMO calculations, the target molecule is divided into units, each of which is called a fragment, and the electronic properties of the target molecule are estimated based on the electronic properties of the monomers and the dimers of the fragments. The specific interactions between the fragments can be investigated based on the interaction energies obtained by the FMO calculations. In the present FMO calculations, each amino acid residue corresponding to a target site on PLN, MMP-9, a selected compound, and individual water molecule were assigned to a fragment, as this fragmentation would allow evaluation of the interaction energies between each residue of the protein and the compound under the effect of water molecules. It should be noted that the Zn ion and some His residues of PLN/MMP-9 were directly coordinated. Therefore, these His residues were considered as part of the same fragment as the Zn ion to precisely describe the coordination bonds among them. Table S2 of SI lists the His residues included in the Zn group for PLN and MMP-9 proteins. In contrast, as Ca ions are not coordinated with the residues of PLN and MMP-9, each Ca ion was considered as a separate fragment. In PLN, Cys31 and Cys58, and Cys270 and Cys297 form disulfide bonds, respectively, and the cysteine pairs forming disulfide bonds were included in the same fragment.

Here we used the MP2/6-31G method [39] of the FMO calculation program ABINIT-MP v6.0 [40] to accurately investigate the π–π stacking, NH–π and CH–π interactions as well as the hydrogen bonding and electrostatic interactions between the PLN/MMP-9 and the compound. In addition, to elucidate which residues contributed to the binding of the compound, we investigated the IFIEs [37] obtained by the FMO calculations. Since metalloproteases PLN and MMP-9 have Zn ions, the convergence of the self-consistent charge in the FMO calculation was very slow. Therefore, we lowered the criteria for the convergence from 0.5×10^{-6} to 0.5×10^{-5} Hartree.

3. Results and discussion

3.1 Stable structures of the PLN/MMP-9 + compound complexes

First, we assigned protonation states of His residues in PLN based on the pKa values predicted by the PROPKA 3.1 program [27, 28]. Since His residues within a protein can either be in the Hid or Hie state, depending on the structure of the surrounding residues, we assigned the protonation state of each His residue considering the steric hindrance produced by the surrounding residues. Table S3 (see SI) lists the pKa values, protonation states, and positions of the His residues in PLN. It is noted, that the Zn ion is coordinated with the nitrogen atoms at the ε-sites of the imidazole rings of both the His140 and His144 residues, and that these coordination bonds do not form if a proton is added to the ε-site. Accordingly, these His residues should possess Hid protonation states. His77 and His224, which are located far from the Zn active site, were assigned the Hie and Hid state, respectively, considering their steric hindrance by Thr39 and the crystal water molecule, as listed in Table S3. In contrast, His223 can either be in the Hid or Hie state, since there is no residue to interact with His223. Therefore, we constructed two structures of PLN with the Hid223 or Hie223 protonation state and docked the compound to both PLN structures. Some of the docked structures were fully optimized in water using the MM method, and finally the total energies of the optimized structures were evaluated precisely by *ab initio* FMO method, to determine a more stable protonation state based on the total energies. As described below, the protonation states of His223 have a significant influence on the structure and the electronic properties around the Zn ion of PLN.

MMP-9 has 11 His residues and their protonation states were assigned uniquely as listed in Table S4 of SI, using the same conditions as for PLN. Particularly, since His175, His190, His203, His226, His230, and His236 are coordinated with one of the two Zn ions in MMP-9, their protonation states were assigned carefully by considering their coordination bonds with the Zn ion. His257 is located near Asp259, and if it has a Hid protonation state, a steric hindrance is caused between Hid257 and Asp259. Accordingly, we assigned the Hie257 protonation state. The other His residues have pKa values higher than six and are located on the surface of MMP-9, so that they were assigned to have the Hip^+ protonation state.

Table 1 lists the results of the simulations of each compound docking to PLN. Here we considered two types of PLN structures, which possess the Hid223 or the Hie223 protonation state. When Compounds 13 and 15 were docked, only two clusters were created by AutoDock, and the top-ranked cluster contained almost all of the created poses. This result indicates that Compounds 13 and 15 prefer to bind certain specific sites of PLN. Although we usually employed the cluster with the largest number of poses in the MM and FMO calculations, here we employed the two clusters and determined a more stable structure based on their total energies evaluated by FMO calculations. As listed in the last column of Table 1, when PLN possesses Hid223, Cluster 2 is more stable, while Cluster 1 is more stable for the PLN with Hie223. Therefore, our docking and FMO results for Compounds 13 and 15 revealed

that the protonation state of His223 in PLN has significant influence on the relative stability among the clusters creased by AutoDock.

In contrast, when Compounds 50 and 51 were docked to PLN, a large number of clusters were created, as presented in Table 1. Among the clusters, we selected those including more than 20 poses, and their representative structures were employed in the subsequent MM and FMO simulations because the larger number of poses in the cluster meant a higher possibility that each compound had one of the conformations of the poses in the cluster. For the PLN (Hid) + Compound 50 complex, Clusters 1, 2, and 3 were employed, and Cluster 3 was found to be the most stable. For the other complexes, the top-ranked Cluster 1 created by AutoDock was found to be the most stable.

In the simulations of the ligand docking to a protein, we usually employed only the top-ranked cluster created by AutoDock. The binding energy (BE) between the protein and ligand is evaluated by the classical MM method in AutoDock and may contain errors, and it is therefore a risk that the ranking of clusters which is based on the BE may be incorrect. In particular, when there is charge transfer between protein and ligand, the BE evaluated by the MM method can cause a significant error because the effect of the charge transfer cannot be considered in the MM method. In contrast, the *ab initio* FMO method can describe the charge transfer and evaluate the BEs precisely. Consequently, we employed certain clusters created by AutoDock and determined the most stable structure based on the total energies evaluated using the FMO method. Table 1 clearly indicates that the top-ranked cluster in AutoDock does not necessarily correspond to the most stable structure in the FMO calculations. This result warrants the need for careful consideration in selecting clusters from AutoDock results.

In the present study, we considered two types of His protonation states for His223 in PLN and investigated which state is more preferable in the PLN + compound complexes using the FMO method. From Table 1a and 1b, we picked up the most stable clusters for each complex and compared their total energies. For the PLN + Compound 15 complex, the structure with Hid223 is 41 kcal/mol more stable than the structure with Hie223. For the other complexes, the structure with Hie223 is at least 22 kcal/mol more stable. This result indicates the possibility that binding of different ligands may induce different protonation states of His223 in PLN. A similar result was predicted in our previous FMO study [22] for the complexes of the vitamin D receptor and its ligands. Therefore, our present FMO calculations reveal that His223 in PLN can be significantly affected by the ligand binding to PLN. In the following calculations, we employed the structures with the more stable protonation state for His223 in PLN.

In the same manner as PLN, the most stable structures for the MMP-9 + compound complexes were determined using the FMO method. As presented in Table 2, when

Compounds 13 and 15 were docked to MMP-9, only one cluster was created by AutoDock, indicating that these compounds had higher binding affinities to a specific site of MMP-9 with similar conformations. In contrast, Compounds 50 and 51 could bind to many different sites of MMP-9. In addition, it was found that Cluster 4 is significantly (291 kcal/mol) more stable than the top-ranked structure for the MMP-9 + Compound 51 complex. Accordingly, we employed the most stable structure for each MMP-9 complex in the following calculations.

3.2 Binding properties between PLN/MMP-9 and compound

To check the adequacy of the present molecular simulations, we first evaluated total IFIEs between each of the compounds and all amino acid residues of PLN using the *ab initio* FMO method. These values are compared with the IC_{50} values obtained through experiments [19] in Table 3. Additionally, as shown in Figure S4 of SI, the correlation between the total IFIEs and the IC_{50} values of the four compounds was analyzed to elucidate that the total IFIEs correlate well with the IC_{50} values. The correlation coefficient (R^2) was 0.94. Accordingly, it is confirmed that our evaluated total IFIEs can explain the trend of the observed binding affinities between PLN and these compounds.

As shown in Figures 1a and 1c, Compounds 13 and 50 contain two Cl atoms at the phenyl ring, and they bind more strongly to PLN rather than MMP-9, as listed in Table 3. Therefore, they are expected to be potent and selective inhibitors of PLN rather than MMP-9. In contrast, as for Compounds 15 and 51, in which the Cl atoms are replaced with F atoms, the sizes of their total IFIEs of PLN are smaller than those of MMP-9, indicating that these compounds prefer to bind to MMP-9, and may cause side effects in humans. Table 3 also indicates that Compound 13 has the largest selective binding to PLN rather than to MMP-9. Accordingly, Compound 13 is expected to be potent and more selective inhibitor to PLN.

To elucidate the cause of the selective binding of Compound 13 to PLN, we investigated the IFIEs between Compound 13 and each of the residues of PLN and MMP-9. As shown in Figure 2a, Compound 13 interacts strongly with the Zn group, Glu141, and Tyr114 of PLN. In particular, the Zn group and Glu141 interact strongly with Compound 13, indicating that they are important sites for strong binding between PLN and Compound 13. In contrast, as shown in Figure 2b, Compound 13 binds strongly with only the Zn1 group of MMP-9. As a result, the total IFIE of MMP-9 is 39 kcal/mol smaller than that of PLN. Therefore, as indicated in Figure 2, Glu141 of PLN is important for selective binding of Compound 13 to PLN in front of MMP-9.

To reveal the reason for the difference in IFIEs of Compound 13 for PLN and MMP-9, we further analyzed the interactions between Compound 13 and some important residues of PLN or MMP-9. As shown in Figure 3a, one of the oxygen atoms of Compound 13 is

coordinated strongly with the Zn ion at 1.9 Å. In addition, the SH group of Compound 13 forms a hydrogen bond with the terminal COO^- group of the Glu141 side chain. This group also interacts electrostatically with the CH group of the phenyl ring in Compound 13, resulting in the significant attractive interaction between Glu141 and Compound 13, as shown in Figure 2a. Compound 13 also interacts electrostatically with Asn112 at 2.6 Å and Tyr155 at 2.8 Å, respectively. These strong interactions between Compound 13 and PLN residues, as well as with the Zn ion, were determined to be the main reason for the strong binding of Compound 13 to PLN.

In the MMP-9 + Compound 13 complex (Figure 3b), one of the oxygen atoms of Compound 13 is coordinated strongly with the Zn ion at 1.9 Å, while the other oxygen atom forms a hydrogen bond with the NH group of the backbone between Leu187 and Leu188. In addition, Compound 13 interacts electrostatically with many MMP-9 residues such as Leu187, Ala189, Hid226, and Tyr248. The phenyl ring of Compound 13 forms a π–π stacking interaction with Hid226. However, there is no MMP-9 residue that interacts strongly with Compound 13 in a similar manner as Glu141 of PLN. As a consequence, the total IFIE between Compound 13 and MMP-9 residues is significantly smaller than the total IFIE between Compound 13 and PLN. In particular, Figure 3a elucidates that the interactions between Compound 13 and the terminal COO^- group of the Glu141 side chain of PLN are essential for enhancing the interaction between Compound 13 and PLN.

Compound 15 has almost the same structure as Compound 13, however the size of its total IFIE is larger than that of Compound 13, as listed in Table 3. To clarify the difference in their interactions with PLN, we compared their IFIEs with the PLN residues in Figure 4a. It was found that Compound 13 interacts more strongly with Glu141, while Compound 15 interacts more strongly with the Zn group of PLN. Totally, the binding affinities of these compounds with PLN are similar to each other. Figure 4b shows the interactions between Compound 15 and some residues of PLN. Although Compound 15 has similar structure as Compound 13, its interactions with PLN residues are significantly different from those (Figure 3a) of Compound 13. In particular, the strong hydrogen bond between the SH group of Compound 13 and the terminal COO^- group of Glu141 is not formed between Compound 15 and Glu141. It is likely that the replacement of Cl atoms in Compound 13 by F atoms reduces the steric hinderance around Compound 13, leading to the change of relative position between Compound 13 and Glu141 and the disappearance of hydrogen bond between Compound 15 and Glu141.

As listed in Table 3, Compound 15 interacts strongly with MMP-9 as well as PLN. Thus, it is likely that Compound 15 can inhibit MMP-9 function to cause a side effect in the human body. To clarify the cause for this strong interaction, we investigated the specific

interactions between Compound 15 and each of the MMP-9 residues using the FMO method. Figure 5a shows the difference in IFIEs between each MMP-9 residue and Compounds 15 and 13, indicating that Compound 15 interacts stronger with the Zn1 group of MMP-9 than Compound 13. This difference is considered as a main reason for the larger total IFIE between Compound 15 and MMP-9 residues. In fact, as shown in Figure 5b, Compound 15 is coordinated at a 2.0 Å distance with the Zn1 ion and interacts strongly with the COO^- group of the Glu227 side chain. Since Glu227 is coordinated with the Zn1 ion and included in the Zn1 group, the IFIE between Compound 15 and the Zn1 group becomes larger. In contrast, Figure 3b indicates that there is no strong interaction between Compound 13 and Glu227, although Compound 13 is strongly coordinated with the Zn1 ion. As a result, the IFIE between the Zn1 group and Compound 13 is significantly smaller than that for Compound 15, as shown in Figure 5a. Therefore, as shown in Figures 3b and 5b, the replacement of two Cl atoms at the phenyl ring of Compound 13 by F atoms causes a significant change in interactions between the Zn1 group and Compounds 13 and 15, resulting in the stronger binding of Compound 15 to human MMP-9. Thus, it can be concluded that Compound 13 is more suitable as a candidate compound with less effect on the MMPs, and perhaps fewer side effects in the human body.

As shown in Figure 1, Compounds 50 and 51 are made by replacing the SH group of Compounds 13 and 15 by the CH_2SH group, respectively. To elucidate the effect of the replacement on the interactions between the compounds and PLN residues, we investigated the IFIEs between PLN residues and Compounds 50 and 51. As indicated in Figure 6a, Compound 50 interacts more strongly with the Zn group and Hie223 than Compound 13. However, the interaction between Compound 13 and Glu141 is significantly (47.1 kcal/mol) reduced by the replacement of the SH group. As a consequence, the total IFIE between Compound 50 and PLN is smaller than that for Compound 13, as listed in Table 3. Compound 50 interacts with the Zn ion and the Glu141 side chain in a similar manner as Compound 13 as shown in Figure 6b. However, there is only one electrostatic interaction between Compound 50 and the COO^- group of Glu141, while Compound 13 (Figure 3a) interacts strongly with both of the two oxygen atoms. As a result, the IFIE between Compound 50 and Glu141 is significantly smaller than that for Compound 13.

Figure 7a shows the difference in IFIEs between PLN residues and Compound 51 or 13, indicating that Glu141 binds weaker to Compound 51. To elucidate the reason for this difference, we investigated the structure of interactions between Compound 51 and PLN residues. As shown in Figure 7b, the two oxygen atoms of the COO^- group of Glu141 interact electrostatically with Compound 51 in a similar manner as Compound 13 (Figure 3a). In contrast, there is no hydrogen bond between the SH group of Compound 51 and the COO^-

group. This bond contributes significantly to the strong interaction between Compound 13 and Glu141, as indicated in Figure 3a. Therefore, it is elucidated that the replacement of the SH group of Compound 13 by the CH_2SH group causes a change in conformation of Compound 13 in the ligand-binding pocket of PLN, resulting in the smaller total IFIE between Compound 51 and PLN.

To elucidate the reason for the significant difference in total IFIEs (Table 3) between MMP-9 and Compounds 15, 50, and 51, we investigated the IFIEs between MMP-9 residues and these compounds. As shown in Figure 8a, Compound 15 interacts very strongly with the Zn1 group, and the Zn2 group has some contribution to the binding between Compound 15 and MMP-9. Compound 50 interacts with MMP-9 in a similar manner as Compound 15. However, Figure 8b elucidates that the size of the IFIE between Compound 50 and the Zn1 group is about half of that for Compound 15. In addition, the size for compound 51 is about a fourth of compound 15, as shown in Figure 8c. Therefore, it is apparent from Figure 8 that the interactions between the Zn1 group of MMP-9 and these compounds significantly depend on the structure of the compound and that Compound 15 has the largest total IFIE because it interacts most strongly with the Zn1 group of MMP-9.

The interaction structures between some important MMP-9 residues and Compounds 15, 50, and 51 are compared to reveal the reason for the difference in IFIEs between the compounds. As shown in Figure 5b, Compound 15 interacts strongly with the Zn1 ion, the Glu227 side chain, and the NH group of the main chain between Leu188 and Ala189. As a result, the two oxygen atoms of Compound 15 significantly contribute to the interactions between Compound 15 and MMP-9 residues. The SH group and an F atom of Compound 15 also contribute to the interactions with MMP-9. In contrast, Figure 9a elucidates that Compound 50 has no interaction with Glu227, although it interacts with Zn1, Leu188, Pro246, and Tyr248. Compound 51 has similar interactions with the MMP-9 residues as Compound 50, as shown in Figure 9b. Therefore, the change in the interaction between Glu227 of MMP-9 and Compounds 15, 50, and 51 was found to be main cause for the larger total IFIE of Compound 15 compared with Compounds 50 and 51.

From the present FMO results shown in Table 3 for the existing Compounds 13, 15, 50, and 51 [19], it is elucidated that Compound 13 is the most suitable candidate for being a selective PLN inhibitor, binding stronger to virulence factor PLN than to the human MMP-9. Accordingly, based on Compound 13, we proposed a novel compound as a selective inhibitor and investigated its binding properties with PLN and MMP-9 in the next section.

3.3 Proposal of novel compound inhibiting specifically PLN

As listed in Table 3, our present FMO calculations revealed that Compound 13 is

more suitable as a selective PLN inhibitor. Therefore, we attempted to propose a novel compound based on Compound 13. Since the previous study [20] indicated that compounds with a hydroxamic acid group has high binding affinity for PLN, we introduced this group into Compound 13 to propose Compound N1, as shown in Figure 1e. A hydroxamic acid group was introduced at the site next to the C=O group of the five-membered ring because the oxygen atom is coordinated with Zn ion of PLN.

We docked Compound N1 to PLN and MMP-9 in the same way as the other compounds to produce several candidate structures of the complexes with these proteins. As for the PLN, we employed the structures with a Hid223 or Hie223 protonation state, and the more stable state was determined based on the total energies evaluated using the FMO method. As listed in Table 4, many clusters were produced for the PLN + N1 complex. For PLN with Hid223, only Cluster 1 had candidate poses numbering larger than 20, and the representable structure of this cluster was employed for the subsequent MM and FMO calculations. In contrast, for the PLN with Hie223, there were five clusters having many candidate poses, and their representative structures were employed. These structures were optimized in water by the MM method, and the total energies (TEs) of the optimized structures were evaluated precisely using the FMO method. As listed in the last column of Table 4, Cluster 1 is the most stable among the five selected structures for PLN with the Hie223 protonation state. To delineate which protonation state of His223 that was more stable, we compared the TEs for the most stable clusters of PLN-Hid and PLN-Hie. The structure of PLN-Hid was found to be only 2.5 kcal/mol more stable than the PLN-Hie structure. In addition, the total IFIEs between N1 and all residues of PLN-Hid was evaluated as −251.7 kcal/mol, whose size was significantly (20.6 kcal/mol) larger than that of PLN-Hie structure. Accordingly, we employed the PLN-Hid structure for the N1 complex in the subsequent interaction analysis.

N1 was also docked to MMP-9 using AutoDock to obtain four different clusters. Since each of them had more than 20 poses, we employed all clusters to elaborate their TEs. As presented in Table 4, Cluster 2 of MMP-9 is at least 111 kcal/mol more stable than the other clusters. Therefore, we employed Cluster 2 for the subsequent interaction analysis.

To estimate the binding affinity of N1 to PLN and MMP-9, we investigated the total IFIEs between N1 and all residues of PLN or MMP-9 using the FMO method and compared the results with those for the existing compounds. As presented in Table 3, N1 binds significantly more strongly to PLN than the existing compounds. Although N1 also binds strongly to MMP-9, the difference in total IFIEs for PLN and MMP-9 is 142 kcal/mol, which is considerably larger than that in the IFIEs for Compound 13. Accordingly, it can be concluded that our proposed N1 may have higher PLN vs. MMP-9 selectivity than Compound 13.

Furthermore, we analyzed the IFIE between N1 and each residue of PLN/MMP-9 to determine the reason for the selective binding of N1. As shown in Figure 10a, N1 binds strongly to the Zn group and Glu141, and the sizes of IFIEs were larger than 70 kcal/mol. Figure 10b shows that the difference in IFIEs for Compounds N1 and 13, indicating that N1 interacts more strongly with the Zn group, Glu141, Arg198, and Tyr114, while Compound 13 interacts strongly with Asp168. As a result, the total IFIE for N1 becomes significantly larger than that for Compound 13. Table S5 of SI summarizes the differences in IFIEs between Compounds N1 and 13. Thus, it is concluded that the introduction of a hydroxamic acid group into Compound 13 enhances the binding of Compound 13 to PLN.

As indicated in Figure 11b, the interactions between MMP-9 residue and Compound 13 are also enhanced significantly by the introduction of a hydroxamic acid group. In particular, Zn1 and Zn2 groups of MMP-9 bind more strongly to Compound N1 compared with Compound 13. However, the enhancement of IFIEs for MMP-9 is considerably smaller than that (Figure 10b) for PLN. As a consequence, the selectivity for PLN, rather than MMP-9, of Compound 13 is enhanced by the introduction of a hydroxamic acid group.

To reveal the reason for the change in IFIEs between PLN/MMP-9 and Compound 13 induced by the introduction of a hydroxamic acid group, we analyzed the interaction structures between the compounds and selected important residues of PLN and MMP-9. As shown in Figure 12a, the hydroxamic acid group of N1 significantly contributes to the interactions of N1 to the Zn ion and Glu141 of PLN. The two oxygen atoms are coordinated with the Zn ion, and the terminal hydroxyl group forms a hydrogen bond with the COO^- group of Glu141. In addition, the other parts of N1 interact electrostatically with many PLN residues such as Arg198, Asn112, and Tyr114, while a π–π stacking interaction is formed between N1 and the imidazole ring of Hid223. As a consequence, the interaction between N1 and PLN becomes significantly stronger than that between Compound 13 and PLN.

As for the interactions between MMP-9 and Compound N1, Figure 12b indicates that the oxygen atom and the hydroxyl group of the introduced hydroxamic acid group form a coordination bond with Zn1 ion and a hydrogen bond with the oxygen atom of the main chain between Ala189 and Hid190, respectively. The SH group of N1 also forms a hydrogen bond with the same oxygen atom. Since Hid190 is coordinated with Zn2 and included in the Zn2 group in the present FMO calculations, the IFIE between Zn2 group and Compound 13 is significantly enlarged by the introduction of the hydroxamic acid group. In addition, there are π–π stacking and electrostatic interactions between N1 and the imidazole ring of Hid226, as shown in Figure 12b. Since Hid226 is included in the Zn1 group, the IFIE between the Zn1 group and N1 is significantly larger than that for Compound 13, as indicated in Figure 11b. It is apparent from Figures 10b and 11b that the introduction of the hydroxamic acid group into

Compound 13 significantly enhances the interactions between Compound 13 and MMP-9 as well as PLN and that the influence is more significant for PLN.

4. Conclusions

In the present molecular simulations based on protein−ligand docking, classical MM optimization, and *ab initio* FMO methods, we investigated the specific interactions between existing compounds and bacterial PLN as well as human MMP-9 to determine the reason for their selectivity for PLN in front of MMP-9. To confirm the adequacy of the present molecular simulations, we first investigated the binding affinity between PLN and the compounds. The total IFIEs between PLN and the compounds evaluated using the FMO method cooperate well with the IC_{50} values obtained thorough the previous experiment [19], with a correlation coefficient (R^2) of 0.94. Accordingly, it is confirmed that our evaluated total IFIEs can explain the trend of the observed binding affinities between PLN and these compounds. The interactions of these compounds with MMP-9 were also investigated in the same manner to elucidate that Compound 13 is more suitable as a selective inhibitor for PLN.

To design more selective PLN inhibitors as putative drugs against bacterial infections with a low risk of side effects in human bodies, we proposed a novel Compound N1 (Figure 1e), consisting of a hydroxamic acid group introduced into Compound 13. N1 was docked to PLN and MMP-9, and its binding properties with both proteins were investigated using the *ab initio* FMO method. The results propose that N1 is a more selective inhibitor for PLN than the existing compounds.

Acknowledgments

This collaboration study was carried out under the official agreement regarding international collaboration studies and the student exchange program between Toyohashi University of Technology and UiT−The Arctic University of Norway. The study was also supported by the international internship program of the Japan Student Services Organization (JASSO), the Nitto Foundation, and the Northern Norway Health Authorities (Helse Nord) (grant number HNF 1514−20).

References

[1] Centers for Disease Control and Prevention. *Antibiotic resistance threats in the United States, 2019*. US Department of Health and Human Services, Centres for Disease Control and Prevention, 2019.

[2] A. Cassini, et al., Attributable deaths and disability-adjusted life-years caused by infections with antibiotic-resistant bacteria in the EU and the European Economic Area in 2015: a population-level modelling analysis, Lancet Infect. Dis., 19, 56–66, 2019.

[3] J. O'Neill, Tackling drug-resistant infections globally: Final report and recommendations, The Review on Antimicrobial Resistance, 1–84, 2016.

[4] G. Cox, G. D. Wright, Intrinsic antibiotic resistance: Mechanisms, origins, challenges and solutions, Int. J. Medical Microbiol., 303, 287–292, 2013.

[5] K. Streeter, M. Katouli, Pseudomonas aeruginosa: A review of their pathogenesis and prevalence in clinical setting and the environment, Infection Epidemiology and Microbiology (Infection Epidemiology and Medicine), 2, 25–32, 2016.

[6] WHO publishes list of bacteria for which new antibiotics are urgently needed. https://www.who.int/news-room/detail/27-02-2017-who-publishes-list-of-bacteria-for-which-new-antibiotics-areurgently-needed (accessed 2021-5-3).

[7] M. T. H. Khan, I. Sylte, Determinants for psychrophilic and thermophilic features of metallopeptidases of the M4 family, In Silico Biol., 9, 105–124, 2009.

[8] O. A. Adekoya, I. Sylte, The thermolysin family (M4) of enzymes: Therapeutic and biotechnological potential, Chem. Biol. Drug Design, 73, 7–16, 2009.

[9] F. Rahman, T.-M. Nguyen, O. A. Adekoya, C. Campestre, P. Tortorella, I. Sylte, and J.-O. Winberg, Inhibition of bacterial and human zincmetalloproteases by bisphosphonate- and catechol-containing compounds, J. Enzyme Inhib. Med. Chem., 36, 819–830, 2021.

[10] S. Sjøli, E. Nuti, C. Camodeca, I. Bilto, A. Rossello, J.-O. Winberg, I. Sylte, O. A. Adekoya, Synthesis, experimental evaluation and molecular modelling of hydroxamate derivatives as zinc metalloproteinase inhibitors, Euro. J. Med. Chem., 108, 141–153, 2016.

[11] O. A. Adekoya, S. Sjøli, Y. Wuxiuer, I. Bilto, S. M. Marques, M. A. Santos, E. Nuti, G. Cercignani, A. Rossello, J.-O. Winberg, I. Sylte, Inhibition of pseudolysin and thermolysin by hydroxamate-based MMP inhibitors, Euro. J. Med. Chem., 89, 340–348, 2015.

[12] M. M. Thayer, K. M. Flaherty, and D. B. McKay, Three-dimensional structure of the elastase of *Pseudomonas aeruginosa* at 1.5 Å resolution, J. Biol. Chem., 266, 2864–2871, 1991.

[13] L. Englert, A. Biela, M. Zayed, A. Heine, D. Hangauer, and G. Klebe, Displacement of disordered water molecules from hydrophobic pocket creates enthalpic signature: Binding of phosphonamidate to the S1'-pocket of thermolysin, Biochim. Biophys. Acta,

1800, 1192–1202, 2010.
[14] S. Chakraborti, M. Mandal, S. Das, A. Mandal and T. Chakraborti, Regulation of matrix metalloproteinases: An overview, Mol. Cell Biochem., 253, 269–285, 2003.
[15] Y. Okada, Localization of matrix metalloproteinase 9 in osteoclasts: Implications for bone resorption, Lab. Invest., 72, 311–322, 1995.
[16] I. Stamenkovic, Matrix metalloproteinases in tumor invasion and metastasis, Seminars in Cancer Biology, 10, 415–433, 2000.
[17] M. Egeblad and Z. Werb, New functions for the matrix metalloproteinases in cancer progression, Nature Rev. Cancer, 2, 161–174, 2002.
[18] C. M. Overall and O. Kleifeld, Validating matrix metalloproteinases as drug targets and anti-targets for cancer therapy, Nature Rev. Cancer, 6, 227–239, 2006.
[19] J. Konstantinovic, S. Yahiaoui, A. Alhayek, J. Haupenthal, E. Schönauer, A. Andreas, A. M. Kany, R. Müller, J. Koehnke, F. K. Berger, M. Bischoff, R. W. Hartmann, H. Brandstetter, A. K. H. Hirsch, N-Aryl-3-mercaptosuccinimides as antivirulence agents targeting *Pseudomonas aeruginosa* elastase and *Clostridium* collagenases, J. Medicinal Chem., 63, 8359–8368, 2020.
[20] A. M. Kany, A. Sikandar, S. Yahiaoui, J. Haupenthal, I. Walter, M. Empting, J. Köhnke, and R. W. Hartmann, Tackling *Pseudomonas aeruginosa* virulence by a hydroxamic acid-based LasB inhibitor, ACS Chem. Biol., 13, 2449–2455, 2018.
[21] C. Antoni, L. Vera, L. Devel, M. P. Catalani, B. Czarny, E. Cassar-Lajeunesse, E. Nuti, A. Rossello, V. Dive, E. A. Stura, Crystallization of bi-functional ligand protein complexes, J. Struct. Biol., 182, 246–254, 2013.
[22] Y. Terauchi, R. Suzuki, R. Takeda, I. Kobayashi, A. Kittaka, M. Takimoto-Kamimura, N. Kurita, Ligand chirality can affect histidine protonation of vitamin-D receptor: Ab initio molecular orbital calculations in water, J. Steroid Biochem. Mol. Biol., 186, 89–95, 2019.
[23] M. T. H. Khan, O. -M. Fuskevag, and I. Sylte, Discovery of potent thermolysin inhibitors using structure based virtual screening and binding assays, J. Med. Chem., 52, 48–61, 2009.
[24] X. Hu, S. Balaz, and W. H. Shelver, A practical approach to docking of zinc metalloproteinase inhibitors, J. Mol. Graph. Model., 22, 293–307, 2004.
[25] M. T. H. Khan, Y. Wuxiuer, and I. Sylte, Binding modes and pharmacophore modelling of thermolysin inhibitors, Mini-Reviews Med. Chem., 12, 515–533, 2012.
[26] T. Ezawa, R. Saito, S. Suzuki, S. Sugiyama, I. Sylte, and N. Kurita, Protonation states of central amino acids in a zinc metalloprotease complexed with inhibitor: Molecular mechanics optimizations and ab initio molecular orbital calculations, Biophys. Chem., 261, 106368, 2020.
[27] C. R. Sondergaard, M. H. M. Olsson, M. Rostkowski, and J. H. Jensen, Improved

treatment of ligands and coupling effects in empirical calculation and rationalization of pKa values, J. Chem. Theory Comput., 7, 2284–2295, 2011.

[28] M. H. M. Olsson, C. R. Sondergaard, M. Rostkowski, and J. H. Jensen, PROPKA3: Consistent treatment of internal and surface residues in empirical pKa predictions, J. Chem. Theory Comput., 7, 525–537, 2011.

[29] M. J. Frisch et al., Gaussian 16, Revision C.01, Gaussian Inc., Wallingford CT, 2016.

[30] C. I. Bayly, P. Cieplak, W. Cornell, P. A. Kollman, A well-behaved electrostatic potential based method using charge restraints for deriving atomic charges: the RESP model, J. Phys. Chem., 97, 10269–10280, 1993.

[31] G. M. Morris, R. Huey, W. Lindstrom, M. F. Sanner, R. K. Belew, D. S. Goodsell, A. J. Olson, Software news and updates AutoDock4 and AutoDockTools4: Automated docking with selective receptor flexibility, J. Comput. Chem., 30, 2785–2791, 2009.

[32] D.A. Case, I. Y. Ben-Shalom, S. R. Brozell, D. S. Cerutti, T. E. Cheatham,III, V. W. D. Cruzeiro, T. A. Darden, R. E. Duke, D. Ghoreishi, M. K. Gilson, H. Gohlke, A. W. Goetz, D. Greene, R. Harris, N. Homeyer, S. Izadi, A. Kovalenko, T. Kurtzman, T. S. Lee, S. LeGra, AMBER 2018, University of California, San Francisco, 2018.

[33] J. A. Maier, C. Martinez, K. Kasavajhala, L. Wickstrom, K. E. Hauser, and C. Simmerling, ff14SB: Improving the accuracy of protein side chain and backbone parameters from ff99SB, J. Chem. Theory Comput., 11, 3696–3713, 2015.

[34] W. L. Jorgensen, J. Chandrasekhar, J. D. Madura, R. W. Impey, and M. L. Klein, Comparison of simple potential functions for simulating liquid water, J. Chem. Phys., 79, 926–935, 1983.

[35] J. Wang, R. M. Wolf, J. W. Caldwell, P. A. Kollman, and D. A. Case, Development and testing of a general amber force field, J. Comput. Chem., 25, 1157–1174, 2004.

[36] D. G. Fedorov, T. Nagata, and K. Kitaura, Exploring chemistry with the fragment molecular orbital method, Phys. Chem. Chem. Phys., 14, 7562–7577, 2012.

[37] K. Fukuzawa, Y. Komeiji, Y. Mochizuki, A. Kato, T. Nakano, and S. Tanaka, Intra- and intermolecular interactions between cyclic-AMP receptor protein and DNA: Ab initio fragment molecular orbital study, J. Comput. Chem., 27, 948–960, 2006.

[38] I. Kobayashi, R. Takeda, K. Shimamura, H. Ishimura, R. Kadoya, K. Kawai, M. Takimoto-Kamimura, and N. Kurita, Specific interactions between androgen receptor and its ligand: Ab initio molecular orbital calculations in water, J. Mole. Graph. Model., 75, 383–389, 2017.

[39] Y. Mochizuki, S. Koikegami, T. Nakano, S. Amari, K. Kitaura, Large scale MP2 calculations with fragment molecular orbital scheme, Chem. Phys. Lett., 396, 473–479, 2004.

[40] Y. Mochizuki, K. Yamashita, T. Nakano, Y. Okiyama, K. Fukuzawa, N. Taguchi, S. Tanaka, Higher-order correlated calculations based on fragment molecular orbital scheme, Theor. Chem. Acc., 130, 515–530, 2011.

Tables and Figures

Table 1 Lowest binding energy (BE: kcal/mol) and number of poses within the clusters obtained by the AutoDock4.2.6 program [31]. The clusters were ranked in the order of BE between PLN and the compound. Total energies (TEs: kcal/mol) for the representative structure within each cluster evaluated using FMO, and relative value (ΔTE) compared with that for the most stable structure.

(a) Hid223 protonation

Compound	Cluster	BE	Poses	TE	ΔTE
13	1	−7.59	245	−79224424.5	23.6
	2	−6.95	11	−79224458.1	0.0
15	1	−6.61	223	−78629377.1	0.0
	2	−6.30	33	−78629329.8	47.3
50	1	−7.86	182	−78580015.3	3.5
	2	−7.08	41	−78579906.9	111.9
	3	−7.05	29	−78580018.8	0.0
	4	−6.55	4	–	–
51	1	−6.88	170	−78128232.5	0.0
	2	−6.82	19	–	–
	3	−6.64	38	−78128220.4	12.1
	4	−6.49	24	−78128203.0	29.5
	5	−6.26	2	–	–
	6	−5.59	1	–	–
	7	−5.44	2	–	–

(b) Hie223 protonation

Compound	Cluster	BE	Poses	TE	ΔTE
13	1	−7.67	246	−79224505.1	0.0
	2	−7.05	10	−79224397.1	108.0
15	1	−6.70	241	−78629335.9	0.0
	2	−6.25	15	−78629325.8	10.1
50	1	−7.92	187	−78580067.0	0.0
	2	−7.10	30	−78579992.4	74.6
	3	−7.00	24	−78580033.6	33.4
	4	−6.96	10	–	–
	5	−6.50	5	–	–
51	1	−7.04	166	−78128254.4	0.0
	2	−6.83	15	–	–
	3	−6.75	68	−78128227.6	26.8
	4	−6.22	6	–	–
	5	−6.12	1	–	–

Table 2 Lowest binding energy (BE: kcal/mol) and number of poses within the clusters obtained by the AutoDock4.2.6 program [31]. The clusters were ranked in the order of BE between MMP-9 and the compound. Total energies (TEs: kcal/mol) for the representative structure within each cluster evaluated using FMO, and relative value (ΔTE) compared with that for the most stable structure.

Compound	Cluster	BE	Poses	TE	ΔTE
13	1	−8.09	256	−47063587.8	−
15	1	−7.61	256	−46611860.0	−
50	1	−8.49	116	−46753760.9	0.0
	2	−7.85	5	−	−
	3	−7.78	62	−46753754.3	6.6
	4	−7.61	52	−46753609.0	150.9
	5	−7.51	12	−	−
	6	−7.38	7	−	−
	7	−7.05	2	−	−
51	1	−6.99	213	−46301762.7	291.2
	2	−6.56	2	−	−
	3	−6.32	3	−	−
	4	−6.19	32	−46302053.9	0.0
	5	−6.06	6	−	−

Table 3 Total inter-fragment interaction energies (IFIEs) (kcal/mol) between each compound and all amino acid residues of PLN/MMP-9 evaluated using the FMO method and IC_{50} (μM) values for PLN obtained through experiments [19]. The total IFIEs for our proposed Compound N1 are also listed for comparison.

Compound	Total IFIE		IC_{50} (μM) for PLN
	PLN	MMP-9	
13	−109.8	−71.0	3.4 ± 0.2
15	−116.6	−126.7	3.5 ± 0.2
50	−102.3	−79.3	5.4 ± 0.7
51	−69.2	−73.7	10.1 ± 1.4
N1	−251.7	−109.4	−

Table 4 Lowest binding energy (BE: kcal/mol) and number of poses within the clusters obtained by AutoDock4.2.6 program [31] for complexes of our proposed Compound N1 with PLN or MMP-9. Total energies (TEs: kcal/mol) for the representative structure within each cluster evaluated using FMO, and relative value (ΔTE) compared with that for the most stable structure. TEs are evaluated for the clusters with more than 20 docking poses.

Protein	Cluster	BE	Poses	TE	ΔTE
PLN-Hid	1	−9.06	232	−79376919.4	–
	2	−7.00	7	–	–
	3	−6.46	4	–	–
	4	−6.28	4	–	–
	5	−6.19	5	–	–
	6	−5.48	2	–	–
	7	−4.80	2	–	–
PLN-Hie	1	−7.53	40	−79376916.9	0.0
	2	−7.01	48	−79376838.1	78.8
	3	−6.19	65	−79376735.7	181.2
	4	−6.15	5	–	–
	5	−5.48	41	−79376776.6	140.3
	6	−5.44	8	–	–
	7	−5.26	26	−79376854.5	62.4
	8	−5.22	17	–	–
	9	−4.53	6	–	–
MMP-9	1	−10.43	89	−46833951.2	111.4
	2	−8.17	23	−46834062.6	0.0
	3	−7.50	91	−46833594.1	468.5
	4	−7.25	53	−46833673.7	388.9

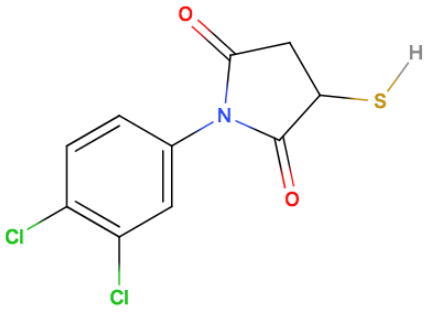

(a) Compound 13

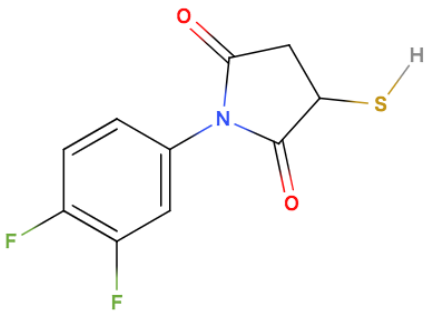

(b) Compound 15

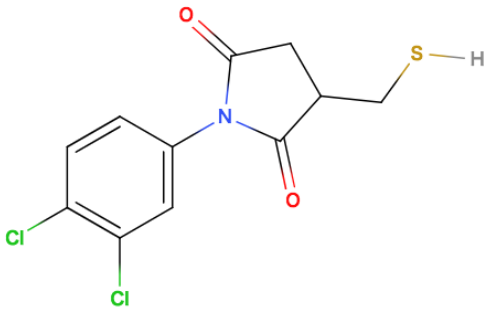

(c) Compound 50

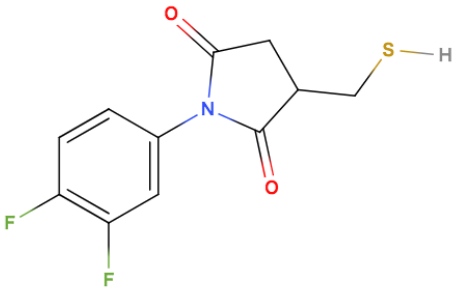

(d) Compound 51

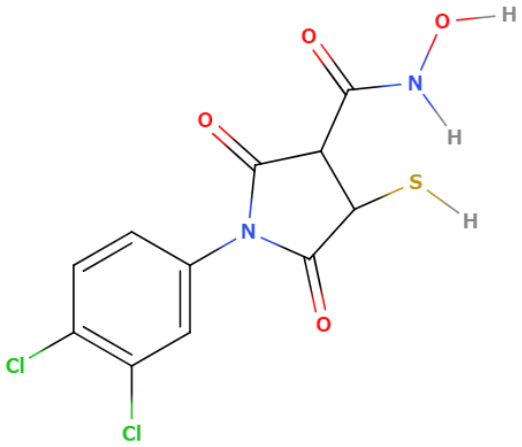

(e) Compound N1

Figure 1 Chemical structures of the existing inhibitors (a–d) for PLN [19] employed in the present study and (e) our proposed novel Compound N1

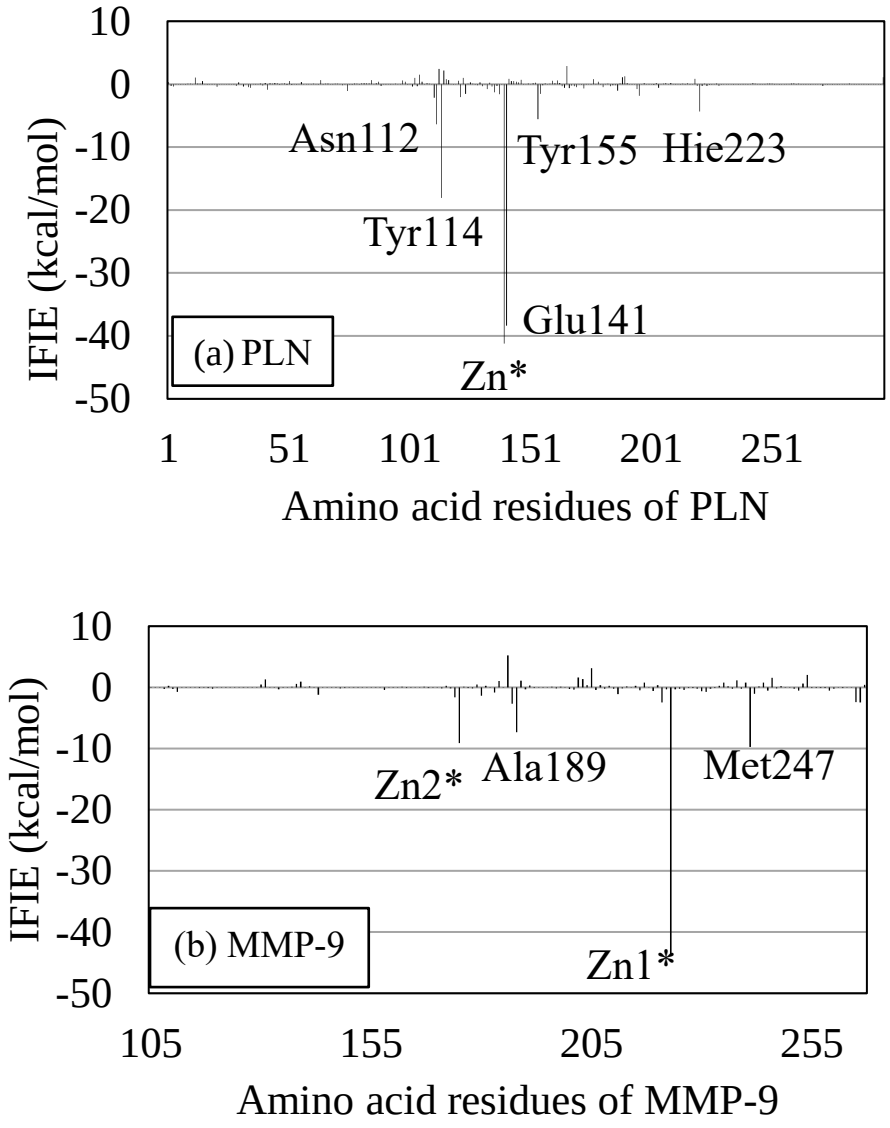

Figure 2 Inter-fragment interaction energies (IFIEs) between Compound 13 and each amino acid residue of (a) PLN and (b) MMP-9. Some important residues interacting strongly with Compound 13 are indicated.

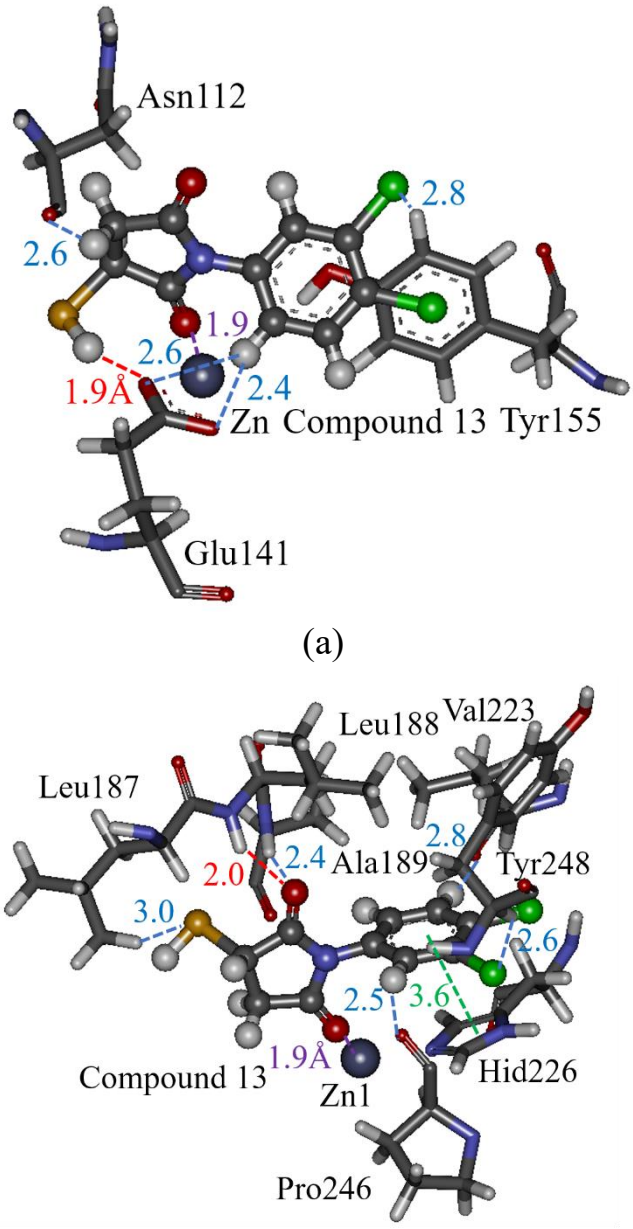

Figure 3 Interactions between Compound 13 (ball-and-stick model) and selected important residues (stick model) in the optimized structure of Compound 13 with (a) PLN and (b) MMP-9. Hydrogen bonding, electrostatic interactions, and π–π stacking interactions, and a coordination bond with Zn are indicated by red, blue, green, and purple lines, respectively.

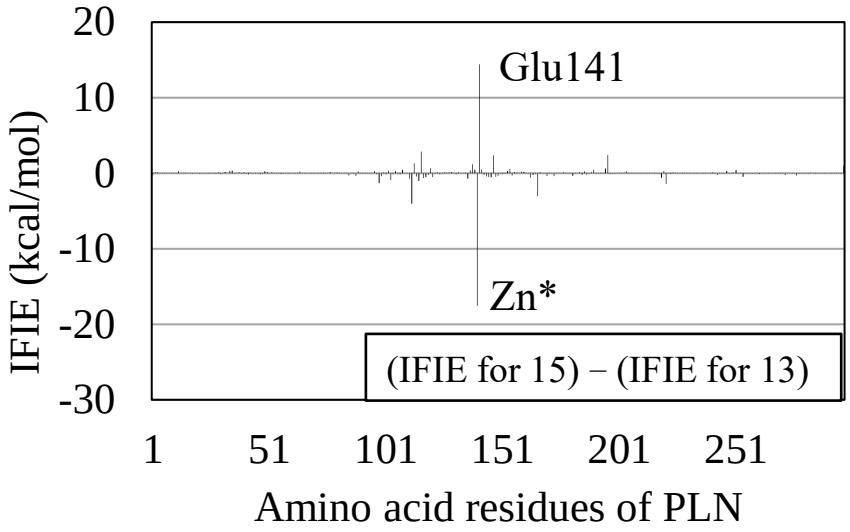

(a)

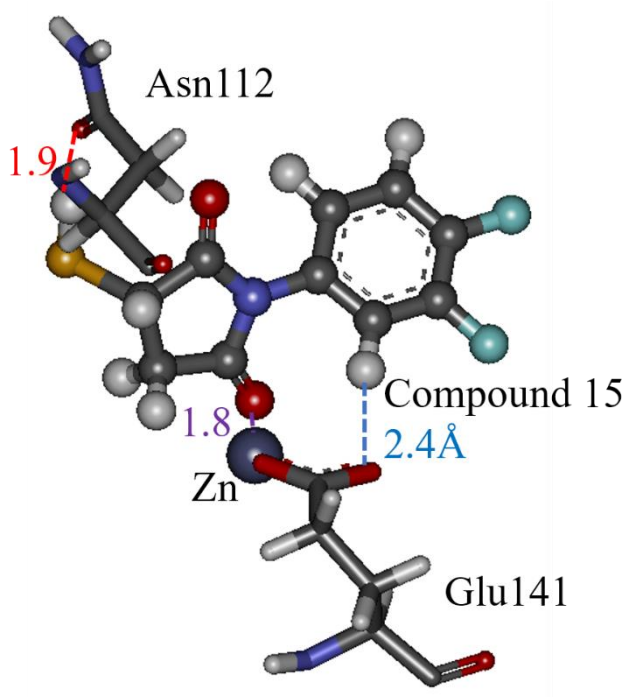

(b)

Figure 4 (a) Difference in the inter-fragment interaction energies (IFIEs) between each PLN residue and Compounds 13 and 15. Glu141 interacts stronger with Compound 13 than Compound 15, while the Zn* group interacts stronger with Compound 15. (b) Interactions between Compound 15 (ball-and-stick model) and selected important PLN residues (stick model) in the optimized complex of PLN + Compound 15. Hydrogen bonding, electrostatic interactions, and a coordination bond with Zn are indicated by red, blue, and purple lines, respectively.

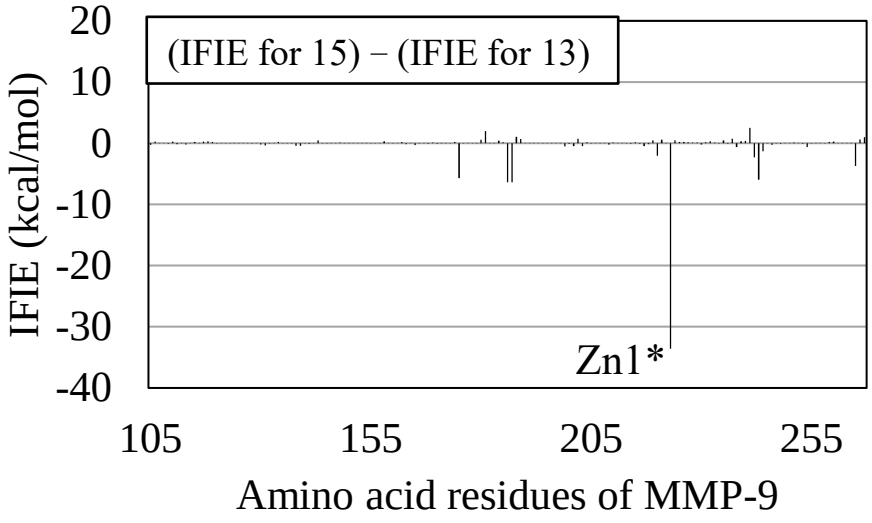

(a)

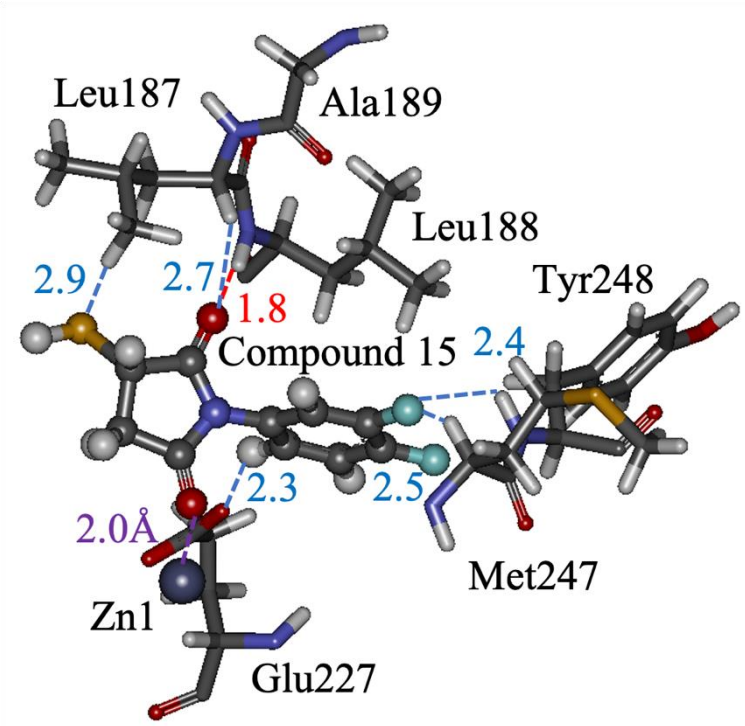

(b)

Figure 5 (a) Difference in the inter-fragment interaction energies (IFIEs) between each MMP-9 residue and Compounds 13 and 15. The Zn1 group interacts stronger with Compound 15 than Compound 13. (b) Interactions between Compound 15 (ball-and-stick model) and selected important MMP-9 residues (stick model) in the optimized complex of MMP-9 + Compound 15. Hydrogen bonding, electrostatic interactions, and a coordination bond with Zn are indicated by red, blue, and purple lines, respectively.

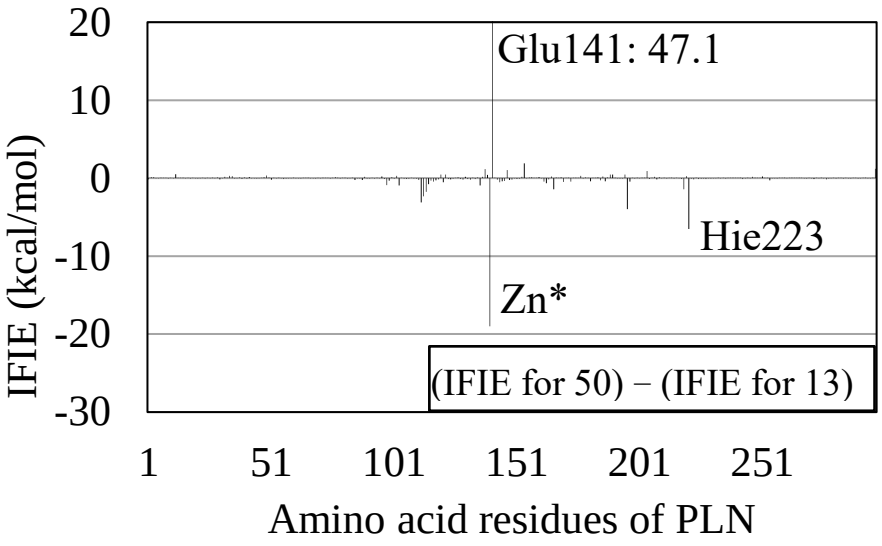

(a)

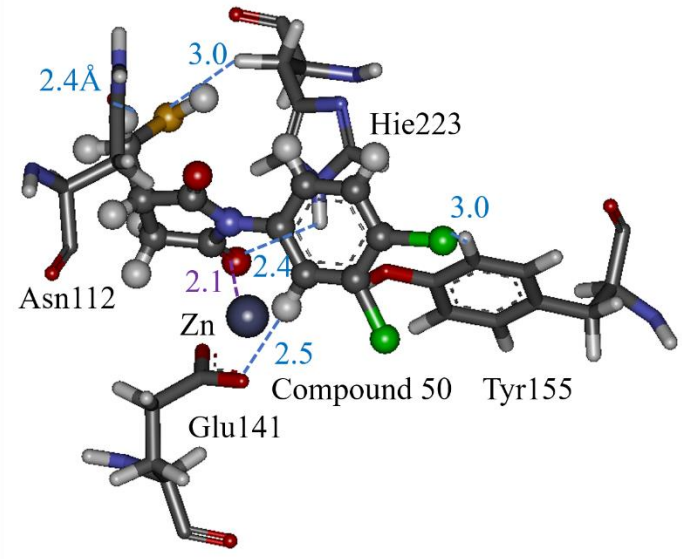

(b)

Figure 6 (a) Difference in the inter-fragment interaction energies (IFIEs) between each PLN residue and Compounds 13 and 50. Glu141 interacts stronger with Compound 13 than Compound 50, while the Zn* group and Hie223 interact stronger with Compound 50. (b) Interactions between Compound 50 (ball-and-stick model) and selected important PLN residues (stick model) in the optimized complex of PLN + Compound 50. Electrostatic interactions and a coordination bond with Zn are indicated by blue and purple lines, respectively.

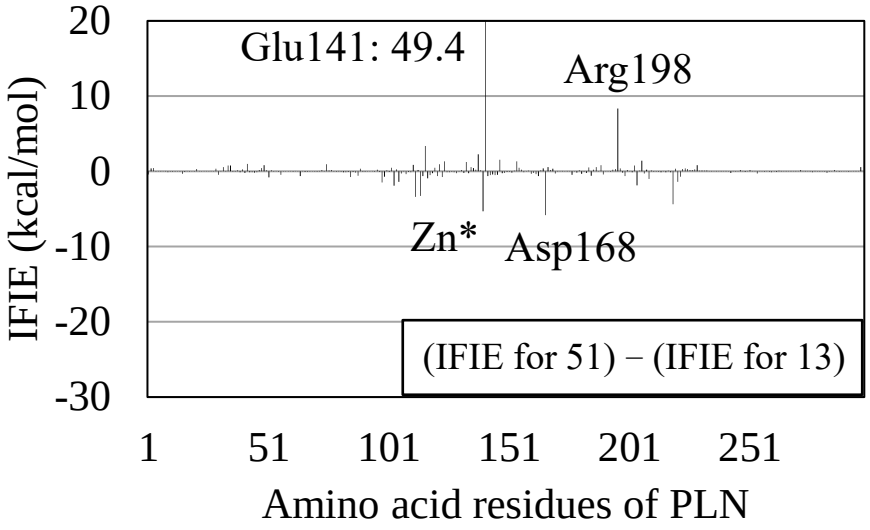

(a)

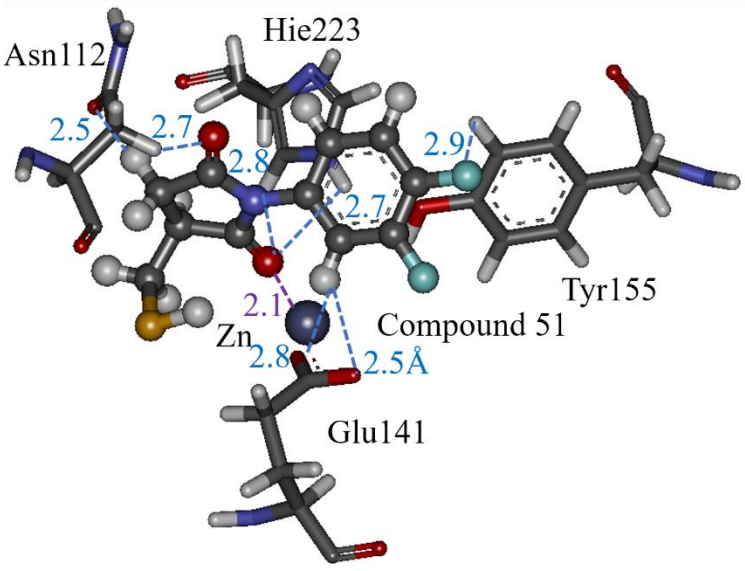

(b)

Figure 7 (a) Difference in inter-fragment interaction energies (IFIEs) between each PLN residue and Compounds 51 and 13. Glu141 and Agr198 interact stronger with Compound 13 than 51, while the Zn group and Asp168 interact stronger with Compound 51. (b) Interactions between Compound 51 (ball-and-stick model) and selected important PLN residues (stick model) in the optimized complex of PLN + Compound 51. Electrostatic interactions and a coordination bond with Zn are indicated by blue and purple lines, respectively.

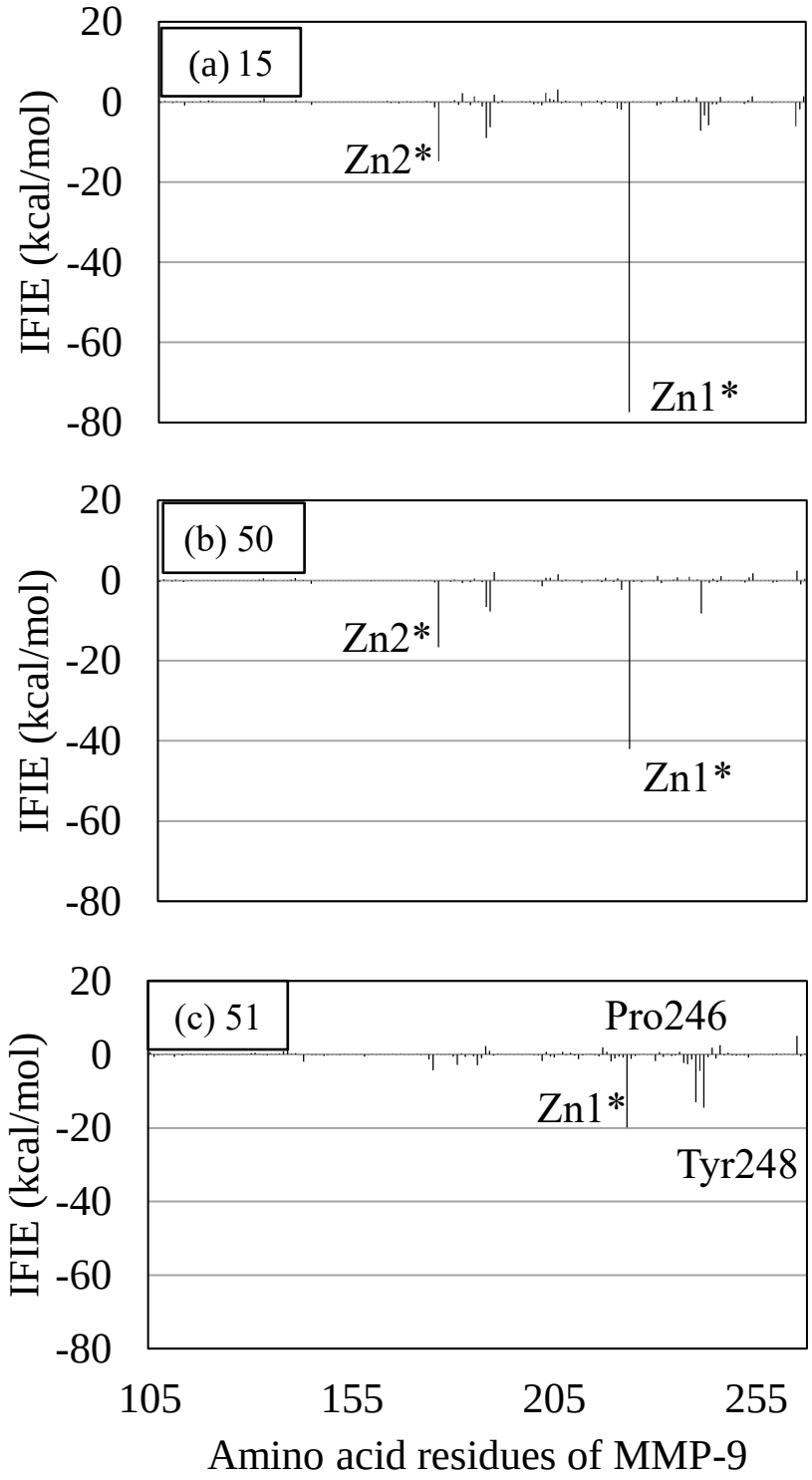

Figure 8 Inter-fragment interaction energies (IFIEs) between amino acid residues of MMP-9 and each of the compounds (a) 15, (b) 50, and (c) 51. Some important residues that interact strongly to the compounds are indicated.

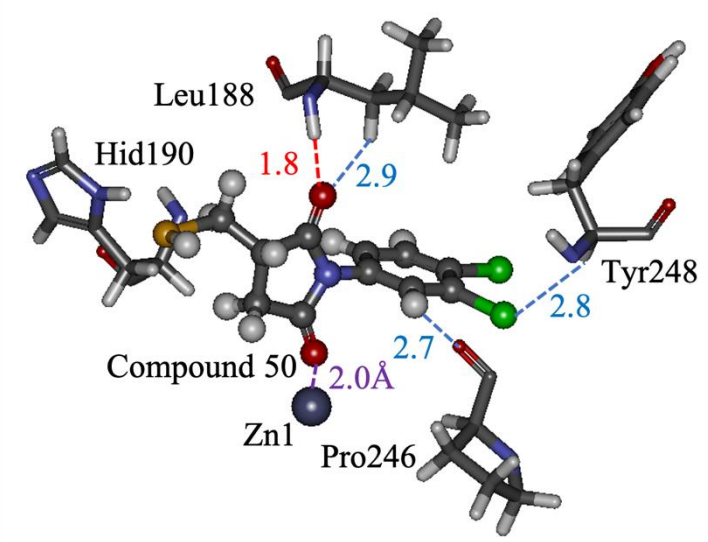

(a)

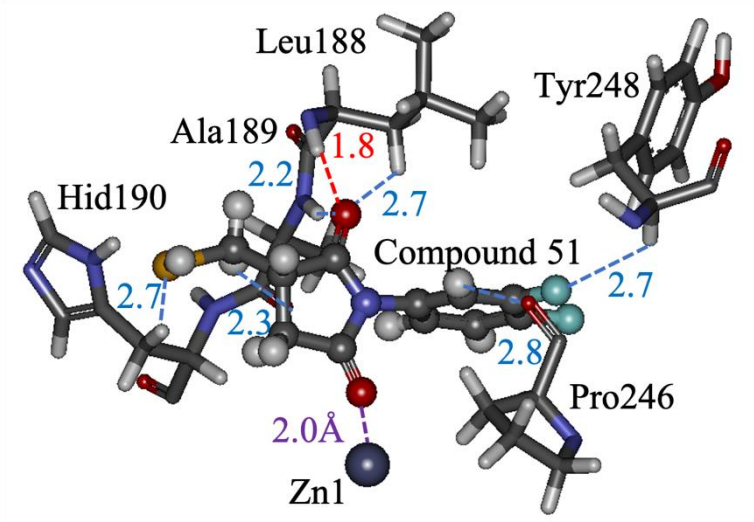

(b)

Figure 9 Interactions between selected important MMP-9 residues (stick model) and (a) Compound 50 (ball-and-stick model) or (b) Compound 51 in the optimized complex of MMP-9 + compound. Hydrogen bonding, electrostatic interactions, and a coordination bond with Zn are indicated by red, blue, and purple lines, respectively.

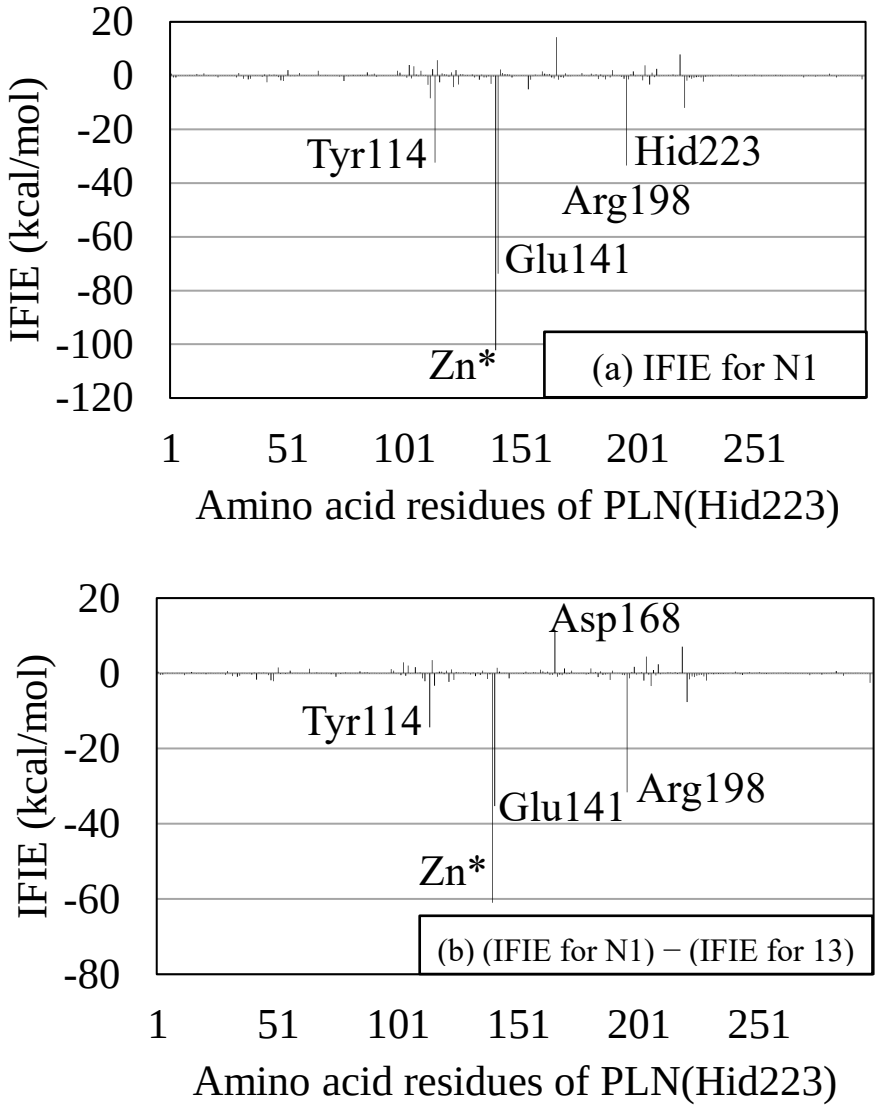

Figure 10 (a) Inter-fragment interaction energies (IFIEs) between Compound N1 and each amino acid residue of PLN with Hid223 protonation state and (b) difference in IFIEs between the compound (13 or N1) and PLN. The Zn* group, Glu141, Arg198, and Tyr114 interact stronger with Compound N1 than Compound 13, while Asp168 interacts stronger with Compound 13.

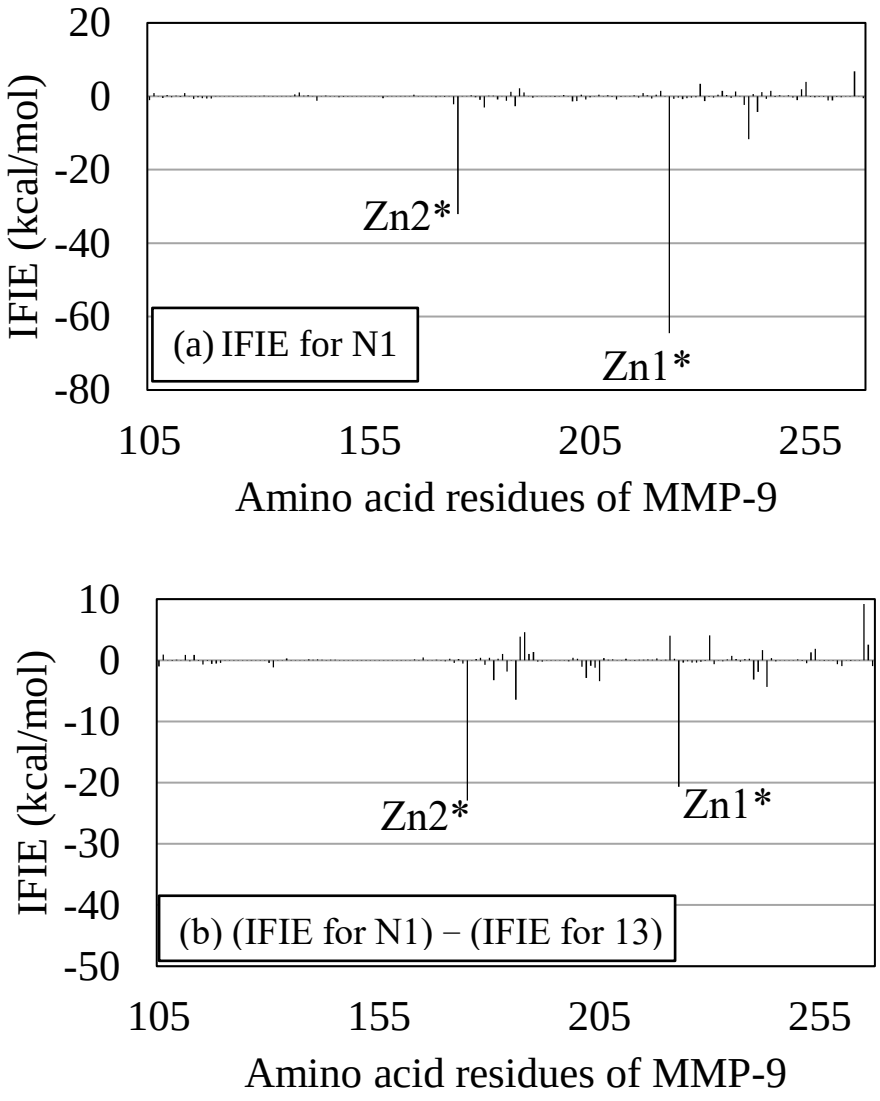

Figure 11 (a) Inter fragment interaction energies (IFIEs) between Compound N1 and each amino acid residue of MMP-9. (b) Difference in IFIEs between each MMP-9 residue and Compounds 13 and N1. The Zn1* and Zn2* groups interact stronger with Compound N1 than Compound 13.

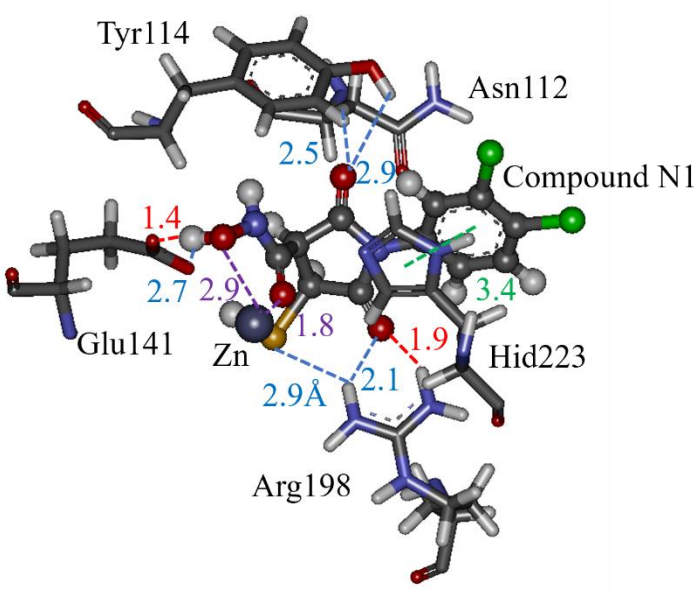

(a) N1 and PLN (Hid223)

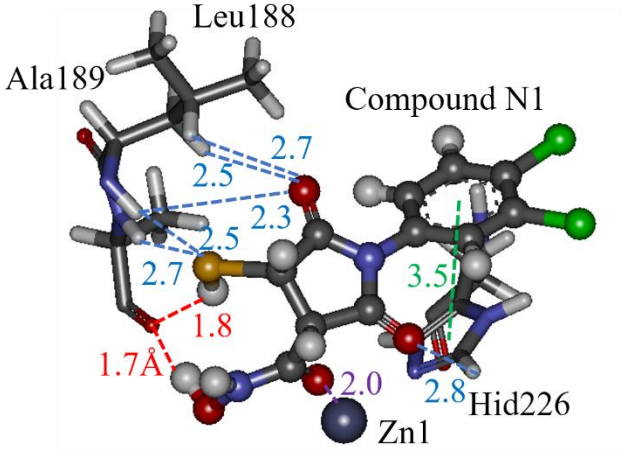

(b) N1 and MMP-9

Figure 12 Interactions between Compound N1 (ball-and-stick model) and selected important residues (stick model) in the optimized complex of Compound N1 with (a) PLN (Hid223) and (b) MMP-9. Hydrogen bonding, electrostatic interactions, and π–π stacking interactions and a coordination bond with Zn are indicated by red, blue, green, and purple lines, respectively.